

Strain-Mediated Magnetization Switching Behavior in a Bicomponent Nanomagnet


Jia-Hui Yuan¹, Xiao-Kuo Yang^{1,*}, Bo Wei¹, Ya-Bo Chen², Huan-Qing Cui¹, Jia-Hao Liu²,
Shu-Qing Dou¹, Ming-Xu Song³ and Li Fei⁴

¹Fundamentals Department, Air Force Engineering University, Xi'an 710051, China

²College of Computer, National University of Defense Technology, Changsha 410005, China

³College of Advanced Interdisciplinary Studies & Hunan Provincial Key Laboratory of Novel Nano-Optoelectronic Information Materials and Devices, National University of Defense Technology, Changsha 410005, China

⁴Aeronautics Engineering College, Air Force Engineering University, Xi'an 710051, China

 (Received 2 May 2022; revised 30 August 2022; accepted 15 November 2022; published 3 January 2023)

The strain-mediated method is considered to be a promising solution for implementing energy-efficient magnetization rotation. However, current methods strictly require a voltage clock. Here, a multiferroic nanomagnet composed of bicomponent magnetic materials (Terfenol-D:Ni = 1:2) is developed to study strain-mediated magnetization switching behavior. With micromagnetic simulations, what is demonstrated is that the strict requirements for a precise applied voltage period can be overcome in such a bicomponent nanomagnet, where the threshold of the square-wave voltage pulse width required for complete and repeated magnetization reversal is only 0.42 ns if the amplitude of the voltage is 1 V. Besides deterministic magnetization switching, further study shows that the unique strain-mediated stochastic magnetization reversal behavior of the designed device can be used to mimic the biological neuron. With the application of the derived neural device parameters, a three-layer artificial neural network is further constructed to recognize a handwritten dataset, based on which, an accuracy of more than 98% can be achieved. Overall, these results open an intriguing way toward straintronic memory and neuromorphic systems.

DOI: [10.1103/PhysRevApplied.19.014003](https://doi.org/10.1103/PhysRevApplied.19.014003)

I. INTRODUCTION

The nanomagnet, a nonvolatile element that can replace the volatile transistor, has attracted much attention from a large number of researchers. Generally, the nanomagnet can be shaped into particular shapes, such as an elliptical disk, the bistable magnetizations of which are encoded as Boolean logic 0 and 1 [1,2]. Through switching the two stable states (0 and 1), information processing can be attained [3,4]. At present, a number of switching mechanisms have emerged, such as magnetic field [5], spin-transfer torque (STT) [6], spin-orbit torque (SOT) [7,8], voltage-controlled magnetic anisotropy [9,10], thermal noise [11,12], microwave [13,14], spin wave [15,16], and strain [17,18]. Among these approaches, voltage-induced strain requires less energy dissipation. Unfortunately, the strain-regulation method reverses the nanomagnet by only 90° [19]. Thus, the auxiliary clock is used to assist straintronics to complete magnetization reversal [20,21]; however, this suffers from device complexity and increases power consumption. To avoid the introduction of an additional clock, Biswas *et al.* achieved magnetization reversal using

two pairs of crossing electrodes fabricated on the piezoelectric layer. However, the voltage is applied to the electrodes in sequence, causing a longer switching time [22,23]. In recent years, the idea of using a precisely timed voltage pulse to obtain 180° magnetization switching has become well known [24–28]. But this kind of method is strictly required for the voltage pulse width. In fact, it is barely possible to apply or withdraw strain at a precise time in the thermal noise.

To alleviate the heavy burden of precise voltage pulse width required by the current strain-mediated magnetization switching methods, a multiferroic nanomagnet composed of a bicomponent nanomagnet is proposed in this paper. For the device, a simulated micromagnetic model is established. Through analyzing the magnetic dynamics of the nanomagnet with different magnetic material proportions, a favorable ratio of Terfenol-D:Ni = 1:2 is selected, motivated by its particular magnetodynamics. The simulation results show that the designed device is able to complete deterministic magnetization switching by feeding with a square-wave voltage pulse of amplitude = 1 V and width ≥ 0.42 ns. Moreover, continuous voltage pulses, which meet the same conditions, can also rotate the magnetization of a nanomagnet in reverse by 180°

*yangxk0123@163.com

repeatedly, whether or not the device is at room temperature. Furthermore, apart from complete magnetization rotation, a sigmoidlike activation function based on the stochastic magnetization switching behavior of the device is revealed by changing the amplitude of the applied voltage, meaning its potential can be utilized as an artificial neuron. In this way, a three-layer artificial neural network (ANN) consisting of the designed spin neurons can successfully recognize a handwritten dataset, and the recognition accuracy can reach more than 98% after 100 training epochs. Additionally, it is found that the designed device is more tolerant to fabrication errors when used as a spin neuron.

II. DEVICE STRUCTURE AND OPERATING PRINCIPLE

The designed multiferroic nanomagnet is depicted in Fig. 1. The nanomagnet is made up of two kinds of magnetic materials (Terfenol-D and Ni) with opposite magnetostriction, λ_s . A square-wave voltage, $V(t)$, is applied to the PZT [Pb(Zr_xTi_{1-x})O₃] layer, which generates biaxial strain by the converse piezoelectric effect. Then the strain, which behaves as tensile strain along the minor axis (x axis) and compressive strain along the major axis (y axis), transfers to the nanomagnet to rotate magnetic moments. Because the effect of the biaxial strain functions the same, it is treated as a total uniaxial strain acting on the major axis for approximate calculations. Note that the thickness of the PZT layer is not evenly distributed. PZT under the Ni part, $h_{\text{Ni-PZT}}$, is thicker than that under the Terfenol-D part, $h_{\text{TD-PZT}}$. The reason is that the voltage is applied simultaneously. Considering the different Young's modulus values of the two materials, the thickness of the PZT layer should be tailored so that the same strain, σ , can be transferred to the Terfenol-D part and Ni part. According to Eq. (1) [18], the ratio of $h_{\text{TD-PZT}}$ to $h_{\text{Ni-PZT}}$ is equal to $Y_{\text{TD}}/Y_{\text{Ni}} = 1:2.675$, so we set $h_{\text{TD-PZT}}$ to 100 nm and $h_{\text{Ni-PZT}}$ to 267.5 nm:

$$\sigma = \frac{YVd_{31}}{h_{\text{PZT}}}, \quad (1)$$

where $d_{31} \approx -10^{-10}$ m/V. Concrete material parameters are given in Table I [29,30]. It is known that, if the product of λ_s and σ is negative, the voltage will generate compressive strain and vice versa [30]. The stress anisotropy constant, K_σ , is used to describe this characteristic [31]:

$$K_\sigma = 3/2\lambda_s\sigma. \quad (2)$$

In other words, if the value of K_σ is negative, the applied voltage performs compressive strain, rotating the magnetic moments by 90°.

On the basis of Eqs. (1) and (2), the operating principle of the designed device can be described as follows: positive voltage generates negative strain, which can rotate

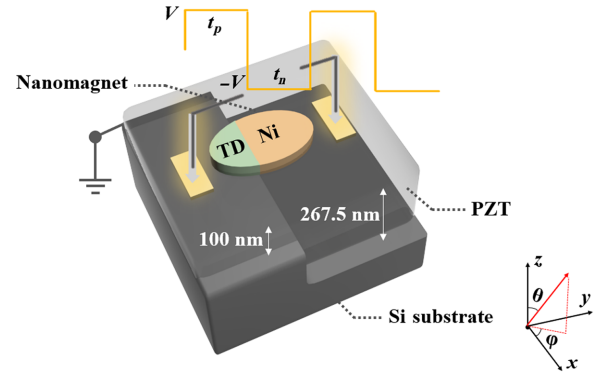


FIG. 1. Schematic illustration of the designed multiferroic nanomagnet. It is mainly composed of three layers: magnetostrictive layer (nanomagnet), piezoelectric layer (PZT), and Si substrate. Nanomagnet consists of Terfenol-D (TD) and Ni materials, and the size is set to $100 \times 120 \times 8 \text{ nm}^3$. Thickness of the PZT layer under the TD part and Ni part is set to 100 and 267.5 nm, respectively. Square-wave voltage pulse (amplitude, V ; positive voltage pulse width, t_p ; negative voltage pulse width, t_n) is applied to the device, making magnetic moments in the nanomagnet complete magnetization switching. φ is the azimuth (in-plane) angle, and θ is the polar (out-plane) angle of the magnetic moment.

magnetic moments in the Terfenol-D part because of its positive magnetostriction. Although magnetic moments in the Ni part cannot rotate under negative strain, they can follow those in the Terfenol-D part through the magnetization interaction between the two parts. In a similar vein, when voltage polarity is reversed, positive strain is produced, which can make the magnetic moments in the Ni part flip. Similarly, the magnetic moments in the Terfenol-D part can rotate under the influence of the Ni part. Thus, if a voltage pulse shaped like that in Fig. 1 is applied to the PZT layer, the device has the potential to complete deterministic magnetization switching under the voltage with changing polarity, which indicates that the magnetization interaction is an essential aid during the switching process. Obviously, an excess Terfenol-D part or Ni part is infeasible for making the nanomagnet undergo magnetization reversal. Therefore, a suitable magnetic material ratio is essential to start subsequent research.

TABLE I. Material parameters.

	Terfenol-D	Ni
Young's modulus, Y (Pa)	8×10^{10}	2.14×10^{11}
Magnetostriction, λ_s	$+6 \times 10^{-4}$	-2×10^{-5}
Gilbert damping constant, α	0.1	0.045
Saturation magnetization, M_S (A/m)	8×10^5	4.85×10^5
Exchange constant, A (J/m)	9×10^{-12}	1.05×10^{-11}

III. DETERMINISTIC MAGNETIZATION SWITCHING

The temporal evolution of the magnetic moment, \mathbf{m} , is solved by the Landau-Lifshitz-Gilbert (LLG) equation [32]:

$$\frac{d\mathbf{m}}{dt} = -\gamma \mathbf{m} \mathbf{H}_{\text{eff}} - \alpha \gamma [\mathbf{m}(\mathbf{m} \mathbf{H}_{\text{eff}})], \quad (3)$$

where $\gamma = 2.21 \times 10^5$ rad/(sT) is the gyromagnetic ratio and \mathbf{H}_{eff} is the effective field applied to the nanomagnet consisting of shape anisotropy, stress anisotropy, thermal fluctuation field, etc. We use the MuMax3 software to simulate the magnetic dynamics [33], assuming a voltage (+1 V, i.e., -80 MPa) is applied on the PZT layer for 2 ns first. Because the magnetization interaction plays a role in the switching process, the necessary voltage amplitude is relatively lower than that in previous studies under the same conditions if the nanomagnet is only made up of Ni [27,34]. Additionally, the magnetostrictive materials are in the polycrystalline state, so their magnetocrystalline anisotropy can be neglected during the simulation [35]. Furthermore, the interface exchange-coupling function is simulated by setting the exchange constant between the two parts as the harmonic mean of the two magnetic materials [36]. Thermal noise is simulated using the RK45 solver with a fixed time step of 10^{-13} s at 300 K [37,38].

A series of material proportions are selected for study. The spatial discretization used for the mesh is 4 nm, which is smaller than the mean exchange length of the two materials. Figure 2 shows the in-plane magnetization-dynamics simulation results, from which it can be seen that, if the nanomagnet is composed of all Ni material or if Terfenol-D:Ni is 1:4, the magnetic moments cannot rotate 90° . Because there is little Terfenol-D in the nanomagnet, this results in the generated compressive strain being too small to drive the magnetic moments. With a greater proportion of Terfenol-D, the magnetic moments can reverse (or more than) 90° . An attractive phenomenon is also observed: the magnetic moments do not return to their initial state (or turn into the opposite state) after the voltage is removed at $t=2$ ns, except for the nanomagnet with all Terfenol-D or Ni material. Particularly for Terfenol-D:Ni = 1:2, the magnetic moments stay beyond $\varphi = 0^\circ$, even though the positive voltage is withdrawn. This illustrates that, if a negative voltage continues to be applied at that moment, a nanomagnet with such a material ratio can complete 180° magnetization reversal under the function of the Ni part.

To verify inference, the dynamic magnetization curve of the nanomagnet with Terfenol-D:Ni = 1:2 is drawn, as depicted in Fig. 3. Its in-plane magnetization rotates over 90° after $t \geq 0.42$ ns. So, according to our assumption, as long as the positive voltage is removed at any time after 0.42 ns and a negative voltage is continuously applied, the nanomagnet will implement 180° magnetization switching

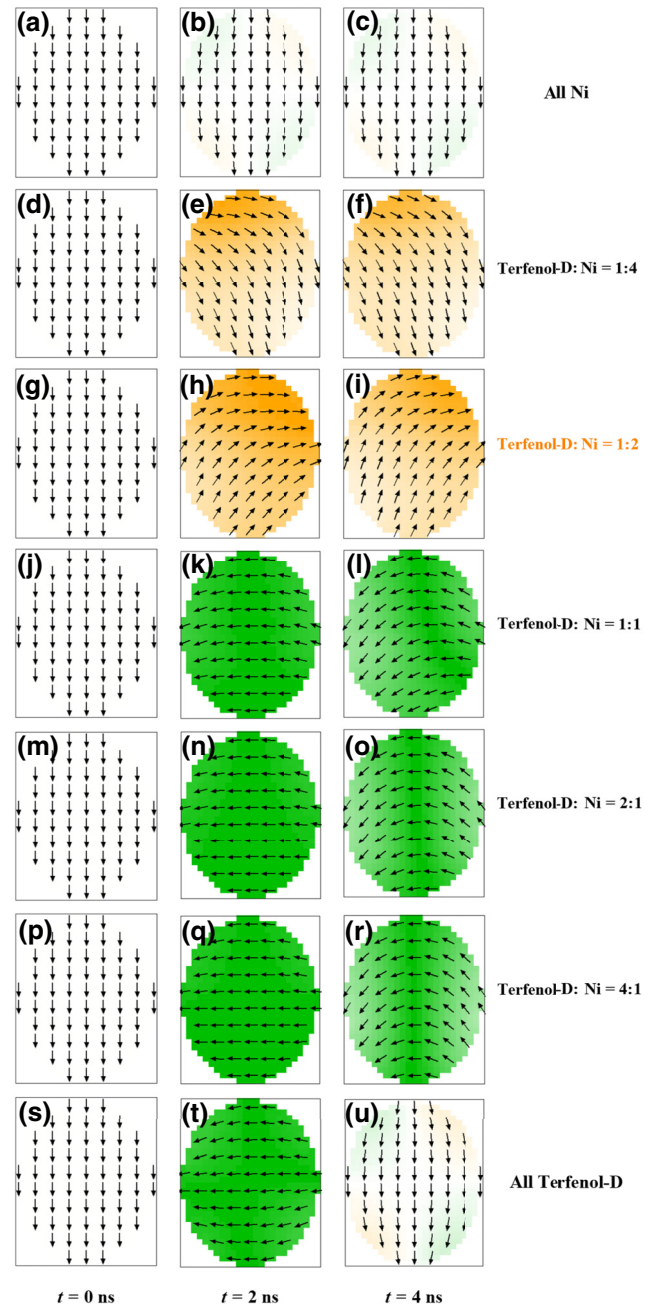


FIG. 2. Initial state of the nanomagnet is set to $\varphi = -90^\circ$. Positive voltage (+1 V, i.e., -80 MPa) is applied to the PZT layer and removed at $t=2$ ns. Nanomagnet comprises different material ratios. (a)–(c) All Ni. Magnetic moments cannot rotate. (d)–(f) Terfenol-D:Ni = 1:4. Magnetic moments cannot rotate 90° . Because there is little Terfenol-D in the nanomagnet, voltage-generated compressive strain is far less than tensile strain. (g)–(i) Terfenol-D:Ni = 1:2. Magnetic moments can rotate over 90° . (j)–(l), (m)–(o), and (p)–(r) Terfenol-D:Ni = 1:1, 2:1, and 4:1, respectively. Magnetic moments can rotate 90° under strain. Among these ratios, when the material ratio is 1:4, 1:2, 1:1, 2:1, and 4:1, the magnetic moments do not return to their initial state after the voltage is withdrawn. (s)–(u) All Terfenol-D. Magnetic moments rotate 90° and then go back to -90° .

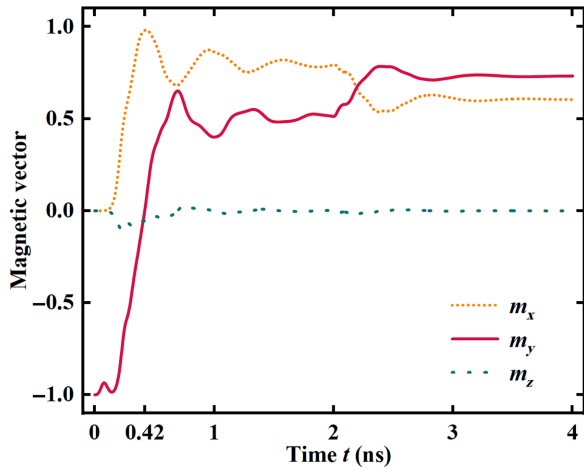


FIG. 3. Dynamic magnetization curve of the nanomagnet composed of Terfenol-D:Ni = 1:2. Magnetization first reaches the “null” state at $t = 0.42$ ns, and then it stays beyond $\varphi = 0^\circ$, even though the voltage is removed at $t = 2$ ns.

behavior. We assume a positive voltage width, $t_p = 0.5$, 1.0, and 2.0 ns, for demonstration. t_n is the width of the negative voltage, which should be long enough to guarantee continued rotation. For the sake of simplicity, it is set equal to t_p here. After micromagnetic simulation, magnetization can rotate 180° in all three cases, showing the correctness of our assumption (Fig. 4).

Except for deterministic magnetization switching, repeated rotation can also be witnessed. With continuous voltage pulses, such as $t_p = t_n = 0.5$ ns, the magnetization of the nanomagnet can reverse at a period of 1 ns, which is the same as the period of the applied voltage [Fig. 5(a)]. Fortunately, the applied clock needs no adjustment, even if the device works at room temperature (300 K) [Fig. 5(b)]. It shows that this way is superior to methods in previous works, the voltage duration times of which should be continually modulated due to the impact of thermal noise [24–27]. In addition, if errors occasionally occur in the voltage pulse width, they cannot affect magnetization switching provided $t_p \geq 0.42$ ns. For example, if the voltage pulse width becomes 2 ns subject to external influence, repeated magnetization switching is also obtained [Fig. 5(d)]. Besides a square-wave voltage, a sinusoidal time-varying voltage can also make the designed device achieve repeated 180° magnetization switching under the condition that the frequency is not more than $f_{\max} = 1/(0.42 \text{ ns} \times 2) \approx 1.2$ GHz. Moreover, the necessary voltage amplitude is minor, as explained in detail in Ref. [17]. But considering the integrality of this paper, we still apply the square-wave voltage clock in the following study.

It is known that the designed device can be fabricated through micro- and nanofabrication technologies, including photoetching, etching, coating, and peeling [39,40].

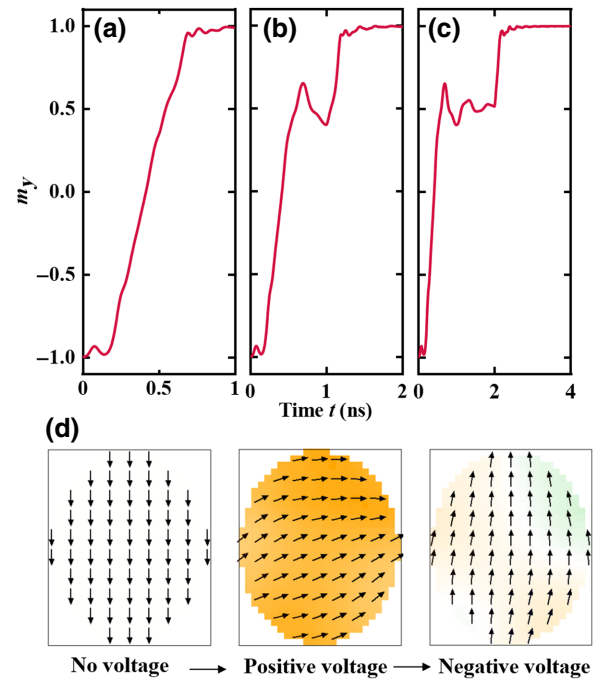


FIG. 4. Nanomagnet with Terfenol-D:Ni = 1:2 achieves 180° magnetization switching successfully when the applied voltage pulse shapes as $V = 1$ V, $t_p \geq 0.42$ ns. (a) $t_p = t_n = 0.5$ ns. (b) $t_p = t_n = 1$ ns. (c) $t_p = t_n = 2$ ns. (d) Gradual variation of magnetic moments under the appropriate applied voltage.

In reality, manufacturing errors always occur and produce deleterious effects on strain-mediated magnetization switching, particularly for memory functions [17,41–44]. These fabrication errors, such as the nonideal boundary of the device, can be alleviated by the bilayer resist technique. But the effect of unavoidable errors such as intrinsic material defects, material ratio errors, and size errors of the nanomagnet should be further studied. The nanomagnet, the size of which is $100 \times 120 \times 8 \text{ nm}^3$ with a material ratio of 1:2, is utilized as a sample for comparison.

How the intrinsic material defects affect the magnetization switching behavior is investigated first. We refer to the simulation methods in Ref. [42] to include intrinsic material defects by setting a rectangle of $8 \times 8 \text{ nm}^2$ in the center of the Terfenol-D or Ni regions. The saturation magnetization of the defective region is set to 50% of the corresponding material. For intrinsic defects in the Terfenol-D part, we apply a voltage of $V = 1$ V for 2 ns and get its threshold voltage-pulse duration time, $t_{\text{th}} = 0.4$ ns, to be slightly shorter than that of the defect-free device (0.42 ns). The minimum strain, $|\sigma|$, to drive magnetization is 27 MPa, which is also smaller than that of the perfect nanomagnet (29 MPa). Similar to defects in the Terfenol-D part, we obtain $t_{\text{th}} = 1.45$ ns, and the minimum strain $|\sigma|$ is 17 MPa when the defects are in the Ni region. Therefore,

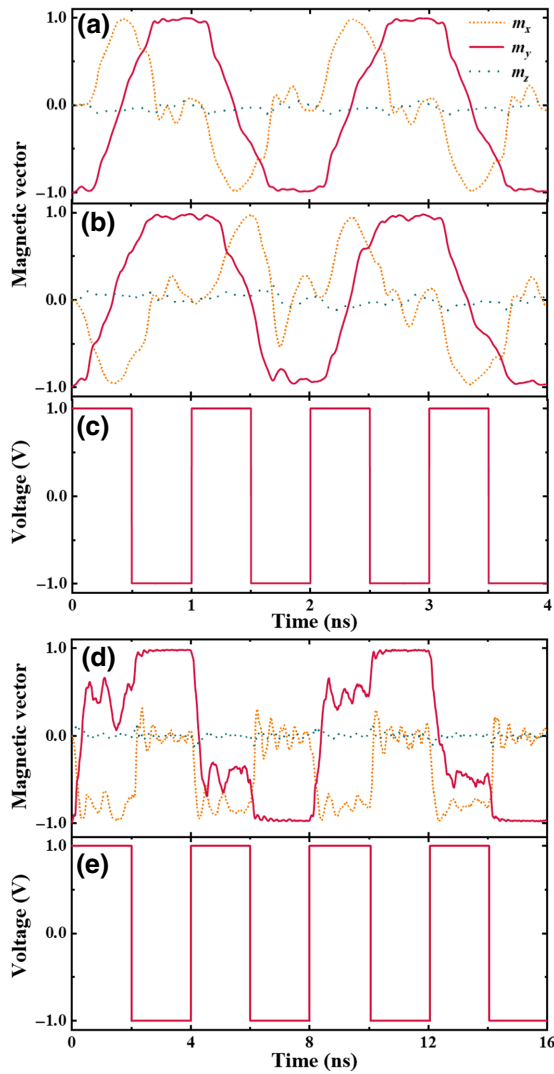


FIG. 5. (a)–(c) Repeated magnetization switching is achieved at (a) 0 K or (b) 300 K when applying identical continuous voltage pulses ($V = 1$ V, $t_p = t_n = 0.5$ ns). (d),(e) If the applied voltage width changes from 0.5 ns to other values, as long as ≥ 0.42 ns, magnetization can still rotate repeatedly ($V = 1$ V, $t_p = t_n = 2$ ns).

intrinsic defects, whether in the Terfenol-D or Ni material, all affect the switching time and strain amplitude of the device. But the impact is not catastrophic and can be modified by adjusting the external clock.

The material ratio error is considered as follows. Table II shows that, as the ratio decreases, namely, the Ni material accounts for more and the Terfenol-D less, t_{th} and $|\sigma|$ gradually increase, resulting in greater energy consumption. And the t_{th} at 300 K is shorter than that at 0 K. This suggests that, if the applied voltage pulse width satisfies the condition at 0 K, it also does at 300 K, as illustrated in Figs. 5(a)–5(c). More importantly, the same square-wave voltage clock with $V = 1$ V, $t_p = t_n = 0.5$ ns, is applied to verify whether the device with material ratio errors can still

achieve 180° magnetization switching. It can be seen from Table II that the nanomagnet with material ratios between 1:2.5 and 1:1.7 fit the conclusion that, if $t_p \geq t_{th}$, the device can complete magnetization rotation. While if the material ratio ranges from 1:1.7 to 1:1.5, the device has already lost the characteristic, as depicted in Figs. 2(g)–2(i), leading to no t_{th} of the device. Nevertheless, at these ratios, the magnetization of the nanomagnet oscillates around the null state under the external clock and rotates exactly over 90° at the moment of 0.5 ns, resulting in the device completing 180° magnetization switching in the next 0.5 ns. Until now, the device is considered to be working under the ideal condition (0 K). Thermal noise should be introduced to confirm the reliability of the designed memory device at room temperature. We simulate 1000 times magnetization switching and record failed rotations, n , of each material ratio under the same clock, representing the probability of switching errors, P_{0° , which can be roughly described using n divided by the total flipping number (1000). We assume an outcome value of normalized magnetization between 0.9 and 1 as successful switching, and other values as failed attempts. The simulation results show that the device with material ratios between 1:2.1 and 1:1.5 has lower switching-error rates. Among these ratios, material ratios between 1:1.7 and 1:1.5 have shorter switching times and smaller stain amplitudes, but they demand a strict voltage pulse width, as previous studies described [25,27], which is at cross purposes to our research. Thus, in terms of switching time, power consumption, and device reliability, material ratios between 1:2.1 and 1:1.9 are more suitable, and it is better to choose 1:2 because of greater error tolerance.

The extended size errors also give rise to switching errors. Using the same simulation approaches as those described above, Tables III–V are obtained, which show the influence of length a , width b , and thickness h , respectively. From Table III, if length a is between 120 to 124 nm, t_{th} is not greater than $t_p = 0.5$ ns, in accordance with $t_p \geq t_{th}$. So, magnetization can reverse successfully. As far as the width effect shown in Table IV is concerned, when width b ranges from 96 to 106 nm, the device can achieve deterministic magnetization switching, since $t_{th} \leq t_p$. When b changes to more than 106 nm, magnetization can still reverse by 180° . This is attributed to the same reason as “when the material ratio is between 1:1.7 and 1:1.5.” Besides, if $b < 95$ nm, the device normally cannot work because the voltage-generated strain is too small to drive magnetization. Similar conclusions can be drawn from Table V. As thickness h varies from 6 to 11 nm, t_{th} gradually increases. When h is between 6 and 10 nm, it satisfies the condition $t_p \geq t_{th}$, showing that the device can achieve deterministic magnetization switching. In addition, when $h < 6$ nm, magnetization rotates by 180° as well. The reason is the same as that for “when width $b > 106$ nm”. If $h > 11$ nm, magnetization cannot rotate by 90° because

TABLE II. Impaction of material ratio on magnetization switching behavior of the designed device.

Material ratio	Threshold of voltage pulse duration, t_{th} (ns)		Minimum strain, $ \sigma $ (MPa)		Magnetization switching or not	Probability of switching errors, P_{0°
	0 K	300 K	0 K	300 K	0 K	300 K
1:1.4	\	\	\	\	✗	1
1:1.5	\	\	22	13	✓	0.052
1:1.7	0.40	\	24	14	✓	0.043
1:1.9	0.42	0.35	29	23	✓	0.07
1:2.0	0.42	0.35	29	23	✓	0.07
1:2.1	0.42	0.35	29	23	✓	0.07
1:2.2	0.45	0.37	43	33	✓	0.271
1:2.5	0.45	0.37	43	33	✓	0.271
1:2.6	0.63	0.40	\	44	✗	0.612

the strain is not strong enough to pull it. Apart from the conditions at 0 K, the device with size errors at room temperature is also taken into consideration. Figure 6 shows the simulation results. From the heat map in Fig. 6(a), we observe that, if the length and thickness of the nanomagnet are constant, there is a key width to minimize magnetization switching errors. Furthermore, as the length gradually increases, the key width grows larger. It is the same when the length of the nanomagnet is fixed [Fig. 6(c)]. On the contrary, if the width is fixed, the key thickness becomes thinner as the length varies [Fig. 6(b)]. In general, from Tables III–V and Fig. 6, it is found that the device has stricter requirements for length than thickness and width. The width and thickness errors are not more than 4 and 2 nm, but only 1-nm length error can negatively influence the deterministic magnetization switching behavior.

IV. STOCHASTIC MAGNETIZATION SWITCHING

The strain-mediated magnetization switching method also has excellent energy superiority for making the artificial neuron, and the switching errors are not too grave in neuromorphic computations. In the past, a straintronic neuron with a steplike activation function was proposed [45]. However, the steplike function is discontinuous and indifferentiable, resulting in difficulty with updating the neural network parameters. To solve the problem, the spintronic neuron with a sigmoidlike activation function

TABLE III. Impact of length a on deterministic magnetization switching behavior of the designed device. (Width, $b = 100$ nm; thickness, $h = 8$ nm; 0 K.)

a (nm)	t_{th} (ns)	Magnetization switching or not
118	\	✗
119	\	✗
120	0.42	✓
122	0.44	✓
124	0.46	✓
126	\	✗

based on the stochastic magnetization switching behavior was studied; this was driven by strain and STT, SOT, or magnetic field [46–48]. This kind of mixed-mode clock still introduces current, increasing power consumption. Similar to deterministic magnetization rotation, the pure voltage-pulse-driven stochastic magnetization switching method was exploited [49]. However, the method suffers from the same disadvantage that the voltage pulse width is demanding. Fortunately, the designed device proposed in this paper solves this problem, as discussed in Sec. III, displaying lower energy consumption and easier regulation of the voltage pulse duration time.

The nanomagnet is still set to $100 \times 120 \times 8$ nm³ and the material ratio is 1:2. To make the magnetization flip randomly, thermal noise is introduced. We feed a square-wave voltage pulse of different amplitudes and the same width (0.5 ns) to the device. The points in Figs. 7(a)–7(c) show the final magnetization-switching-direction distribution for specific $|\sigma|$. The process is repeated 1000 times. As $|\sigma|$ varies, almost no magnetization rotation occurs at $|\sigma| = 10$ MPa, but there is an equal rotation distribution (0° or 180°) at $|\sigma| = 30$ MPa and deterministic switching as $|\sigma|$ changes to 80 MPa, as a consequence of $|\sigma|$ increasing. Additionally, the inset in Fig. 7(e) shows the probability of 180° magnetization switching, $P_{180^\circ} = 1 - P_{0^\circ}$, as $|\sigma|$

TABLE IV. Impact of width b on deterministic magnetization switching behavior of the designed device. (Length, $a = 120$ nm; thickness, $h = 8$ nm; 0 K.)

b (nm)	t_{th} (ns)	Magnetization switching or not
80	\	✗
90	\	✗
95	0.59	✗
96	0.50	✓
100	0.42	✓
106	0.43	✓
107	\	✓
120	\	✓

TABLE V. Impact of thickness h on deterministic magnetization switching behavior of the designed device. (Length, $a = 120$ nm; width, $b = 100$ nm; 0 K.)

h (nm)	t_{th} (ns)	Magnetization switching or not
2	\	✓
4	\	✓
5	\	✓
6	0.39	✓
8	0.42	✓
10	0.50	✓
11	0.56	✗
13	\	✗

is swept from 0 to 80 MPa. The fitted curve exhibits a sigmoidlike activation function, which illustrates that the designed device is expected to be utilized as a spin neuron to perform neuromorphic computations, such as recognizing the Mixed National Institute of Standards and Technology database (MNIST) datasets [50]. Hence, a three-layer ANN composed of the designed device is constructed to testify to its recognition capability [51]. We separately simulate 784, 300, and 10 neurons for the input, hidden, and output layers, as shown in Fig. 7(d). Each digital image in the MNIST dataset includes 28×28 pixels, and every pixel has a gray value in the range of 0–255. The gray value of the picture delivered to the neuron is linearly converted into the voltage amplitude V ($|\sigma|$), and $|\sigma|$ inputted into the network is in the linear region of the activation function, ranging from 20 to 45 MPa. Figure 7(e) shows the neural network training results. After 100 training epochs, the recognition accuracy can reach over 98%, which illustrates that the designed device can be used as an emerging spin neuron that is more energy efficient than traditional artificial neurons.

Considering that fabrication errors give rise to the effect on the magnetization switching behavior, we carry out the following simulation to specify the substantial influence of the material's ratio errors and size errors on the designed spin neuron. The inset in Fig. 8(a) shows that, as the material ratio varies, the analytical fitting function between P_{180° and $|\sigma|$ is changed. Because a material ratio of 1:2.0 behaves the same as material ratios between 1:1.9 and 1:2.1, from Table II, we simulate only the ratio 1:2.0. The material ratio of 1:2.5, which represents the ratio between 1:2.5 and 1:2.2, has lost its sigmoidlike function, indicating that the device cannot perform neuron computations. Figure 8(a) shows the simulated recognition accuracy of the remaining material ratios, except 1:2.5, which can all reach 98% when the inputted $|\sigma|$ is 20–45 MPa. These results indicate that, for a perfect nanomagnet with TD:Ni = 1:2, if the Terfenol-D region accounts for 38–48 nm and the Ni region occupies 72–82 nm along the major axis, there is no detrimental influence on the neuron function. Although material ratios between 1:1.7 and 1:1.5

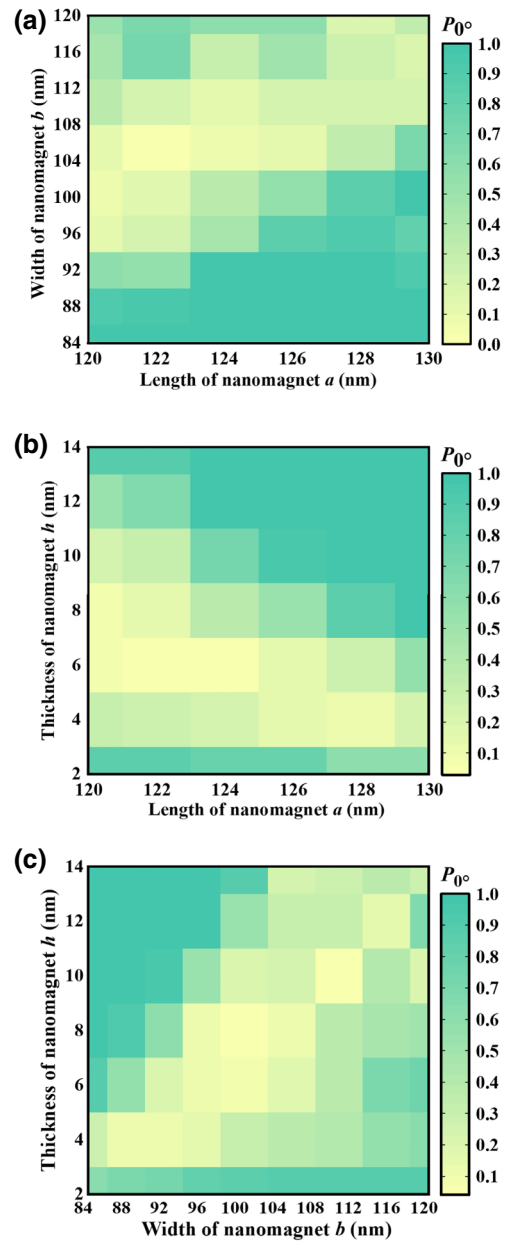


FIG. 6. Probability of switching errors, P_0^o , versus (a) length and width (thickness, 8 nm), (b) length and thickness (width, 100 nm), (c) width and thickness (length, 120 nm) of nanomagnet. Pale yellow fading to dark green represents smaller switching failures varying to larger.

seem to be more suitable, with lower energy consumption and a faster recognition rate, it is not in accordance with the purpose of greater tolerance to the applied voltage duration time, as explained in the discussion of the memory function. So, a material ratio of 1:2.0 is still the best ratio for the designed spin neuron. With the same simulation methods, the impact of size errors is provided, as shown in Figs. 8(b)–8(d). These figures prove that the designed neuron tolerates more size errors than the memory function. For example, the width can tolerate a 4–8-nm

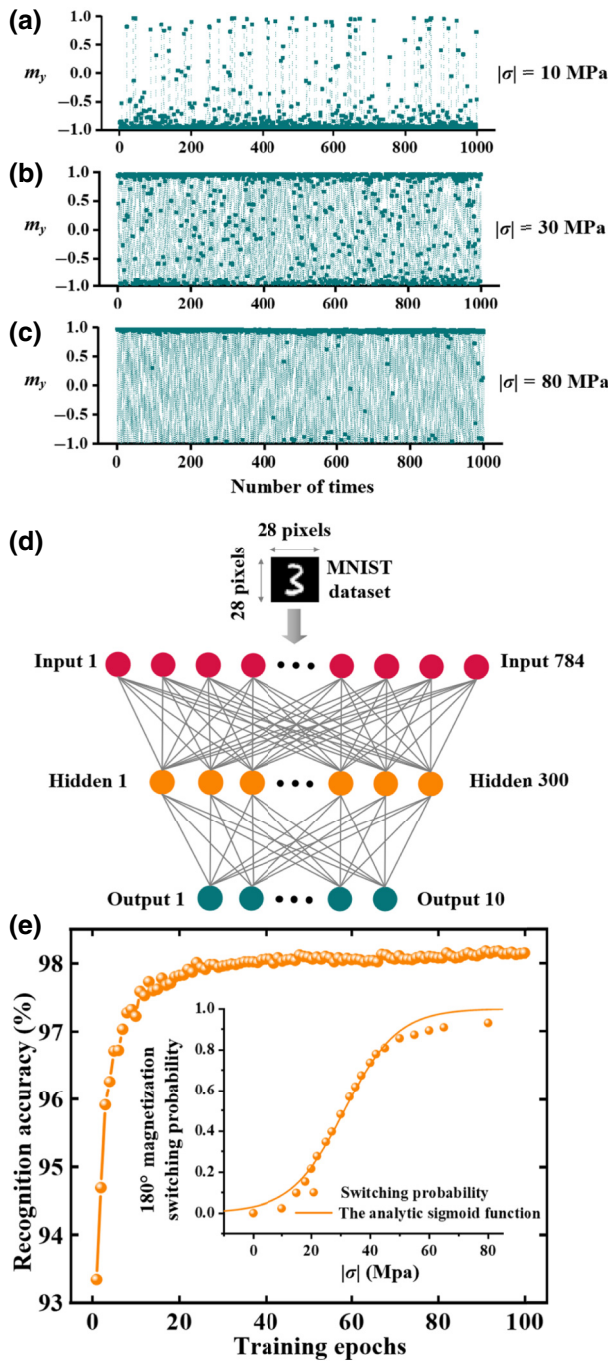


FIG. 7. (a)–(c) Final magnetization-direction distribution of 1000 switching processes under three different applied strain values ($|\sigma| = 10, 30,$ and 80 MPa), showing the number of 180° magnetization switching events as a function of $|\sigma|$. (d) MNIST dataset recognition task is performed by the simulated three-layer ANN. (e) Inset is the 180° magnetization switching probability, P_{180° , as a function of applied strain $|\sigma|$, fitted to sigmoidlike function $y = 1/(1 + e^{-0.11(x-31.28)})$. It can be regarded as the activation function of the designed device. Based on the network composed of the designed neuron, recognition accuracy can reach more than 98% after 100 training epochs.

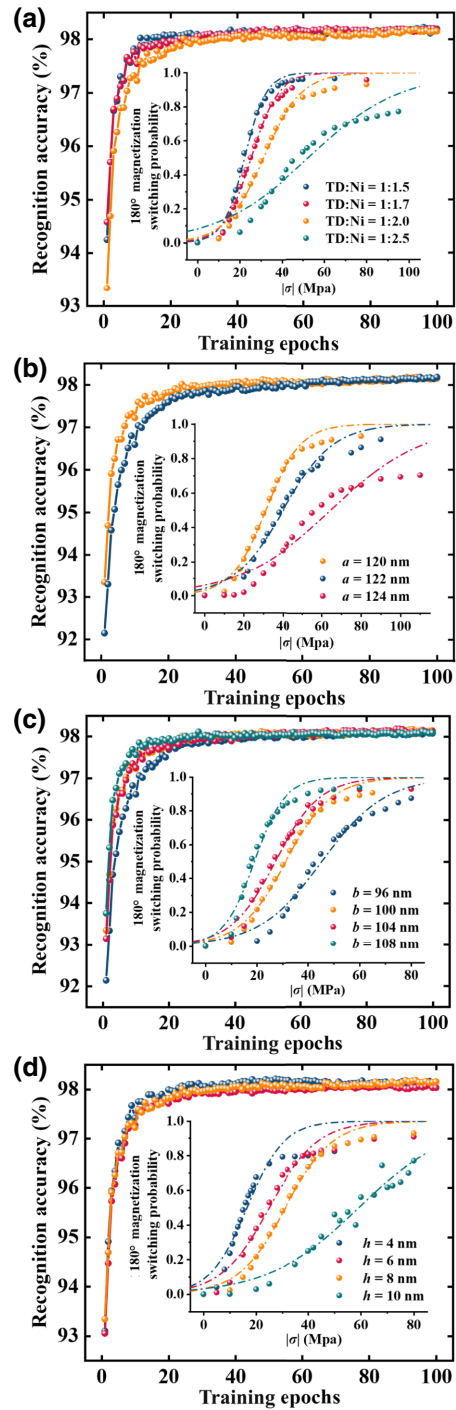


FIG. 8. (a) Recognition accuracy of the network consists of different material ratios of neurons when $|\sigma|$ inputted is between 20 and 45 MPa. Inset, activation functions of different material ratios. (b) With length a extending beyond 2 nm, the device loses the sigmoidlike activation function and recognition ability. (c) When width b of the nanomagnet changes from 96 to 108 nm, the designed device still has the sigmoidlike activation function and can successfully perform the recognition task. (d) $h = 8$ nm is taken for comparison. Thickness can be made 4 nm thinner to maintain the sigmoidlike activation function and recognition ability.

error range, and the thickness can be made 4 nm thinner. Although the results show that the length requirement is still strict and the thickness cannot tolerate more than a 2-nm-thicker error, the dropout layer in the neural network can randomly disable some neurons during the training process. So, disabled devices with size errors can be regarded as discarded neurons, similar to the function of the dropout layer.

V. CONCLUSION

A multiferroic nanomagnet composed of a bicomponent nanomagnet (Terfenol-D: Ni=1:2) is proposed in this paper, which can be applied in memory and neuron devices. It is concluded that deterministic and stochastic magnetization switching behavior can be achieved through the strain-mediated method in the designed device, which shows more tolerance to voltage-pulse-width errors. Specifically speaking, when the amplitude of the applied square-wave voltage is 1 V, all it requires is that the voltage pulse width should be ≥ 0.42 ns for deterministic magnetization reversal, whether or not the device is at room temperature. Additionally, the designed device manifests a smaller necessary voltage amplitude and consumes less energy. After absorbing the merits of the device, the designed device is developed to play a role in the spin neuron, and it can achieve digital recognition successfully. It is believed that the proposed device will advance the fields of energy-efficient straintronic memory and neuromorphic systems.

ACKNOWLEDGMENTS

This work is supported by the National Natural Science Foundation of China (Grant No. 62274183), the Natural Science Basic Research Program of Shaanxi (Grants No. 2022JQ-073 and No. 2021JM-221), the Research Foundation of Fundamentals Department of Air Force Engineering University (Grant No. JK2020203), and the Graduate Scientific Research Foundation of Fundamentals Department of Air Force Engineering University (Grant No. YJS202105). J.-H.Y. and B.W. contributed equally to this work. Y.-B.C. and Q.-H.C established the simulated model. X.-K.Y., J.-H.L, S.-Q.D., M.-X.S., and L.F. discussed the results and modified the manuscript.

-
- [1] R. P. Cowburn, D. K. Koltsov, A. O. Adeyeye, M. E. Welland, and D. M. Tricker, Single-Domain Circular Nanomagnets, *Phys. Rev. Lett.* **83**, 1042 (1999).
 [2] C. Augustine, X. Y. Fong, B. Behin-Aein, and K. Roy, Ultra-low power nanomagnet-based computing: A system-level perspective, *IEEE Trans. Nanotechnol.* **10**, 778 (2011).

- [3] X. K. Yang, L. Cai, B. Zhang, and M. L. Zhang, A mechanism for the crossing of orthogonal magnetic wires in multiferroic nanomagnet logic, *IEEE Trans. Electron Devices* **61**, 487 (2014).
 [4] N. Zhang, B. Zhang, M. Y. Yang, K. M. Cai, Y. Sheng, Y. C. Li, Y. C. Deng, and K. Y. Wang, Progress of electrical control magnetization reversal and domain wall motion, *Acta Phys. Sin.* **66**, 5 (2017).
 [5] G. Csaba, A. Imre, G. H. Bernstein, W. Porod, and V. Metlushko, Nanocomputing by field-coupled nanomagnets, *IEEE Trans. Nanotechnol.* **1**, 209 (2002).
 [6] X. Y. Fong, Y. Kim, K. Yogendra, D. Fan, A. Sengupta, A. Raghunathan, and K. Roy, Spin-transfer torque devices for logic and memory: Prospects and perspectives, *IEEE Trans. CAD* **35**, 1 (2016).
 [7] S. Sayed, S. Hong, E. E. Marinero, and S. Datta, Proposal of a single nano-magnet memory device, *IEEE Electron Device Lett.* **38**, 1665 (2017).
 [8] W. Legrand, R. Ramaswamy, R. Mishra, and H. Yang, Coherent Subnanosecond Switching of Perpendicular Magnetization by the Fieldlike Spin-Orbit Torque without an External Magnetic Field, *Phys. Rev. Appl.* **3**, 064012 (2015).
 [9] P. K. Amiri and K. L. Wang, Voltage-controlled magnetic anisotropy in spintronic devices, *SPIN* **2**, 1240002 (2012).
 [10] W. Kang, Y. Ran, Y. G. Zhang, W. F. Lv, and W. S. Zhao, Modeling and exploration of the voltage-controlled magnetic anisotropy effect for the next-generation low-power and high-speed MRAM applications, *IEEE Trans. Nanotechnol.* **16**, 387 (2017).
 [11] I. L. Prejbeanu, W. Kula, K. Ounadjela, R. C. Sousa, O. Redon, B. Dieny, and J.-P. Nozieres, Thermally assisted switching in exchange-biased storage layer magnetic tunnel junctions, *IEEE Trans. Magn.* **40**, 2625 (2004).
 [12] D. Pinna, A. D. Kent, and D. L. Stein, Thermally assisted spin-transfer torque dynamics in energy space, *Phys. Rev. B* **88**, 104405 (2013).
 [13] J. G. Zhu and Y. M. Wang, Microwave assisted magnetic recording utilizing perpendicular spin torque oscillator with switchable perpendicular electrodes, *IEEE Trans. Magn.* **46**, 751 (2010).
 [14] N. Barros, M. Rassam, and H. Kachkachi, Microwave-assisted switching of a nanomagnet: Analytical determination of the optimal microwave field, *Phys. Rev. B* **88**, 014421 (2013).
 [15] T. Schneider, A. A. Serga, B. Leven, and B. Hillebrands, Realization of spin-wave logic gates, *Appl. Phys. Lett.* **92**, 022505 (2007).
 [16] A. V. Sadovnikov, A. A. Grachev, E. N. Beginin, S. E. Sheshukova, Yu P. Sharaevskii, and S. A. Nikitov, Voltage-Controlled Spin-Wave Coupling in Adjacent Ferromagnetic-Ferroelectric Heterostructures, *Phys. Rev. Appl.* **7**, 014013 (2017).
 [17] D. Winters, M. A. Abeer, S. Sahoo, A. Barman, and S. Bandyopadhyay, Reliability of Magnetoelastic Switching of Nonideal Nanomagnets with Defects: A Case Study for the Viability of Straintronic Logic and Memory, *Phys. Rev. Appl.* **12**, 034010 (2019).
 [18] K. Roy, S. Bandyopadhyay, and J. Atulasimha, Switching dynamics of a magnetostrictive single-domain nanomagnet subjected to stress, *Phys. Rev. B* **83**, 224412 (2011).

- [19] J. Atulasimha and S. Bandyopadhyay, Bennett clocking of nanomagnetic logic using multiferroic single-domain nanomagnets, *Appl. Phys. Lett.* **97**, 173105 (2010).
- [20] A. K. Biswas, S. Bandyopadhyay, and J. Atulasimha, Energy-efficient magnetoelastic non-volatile memory, *Appl. Phys. Lett.* **104**, 232403 (2014).
- [21] Q. C. Wang, J. Domann, G. Q. Yu, A. Barra, K. L. Wang, and G. P. Carman, Strain-Mediated Spin-Orbit-Torque Switching for Magnetic Memory, *Phys. Rev. Appl.* **10**, 034052 (2018).
- [22] A. K. Biswas, S. Bandyopadhyay, and J. Atulasimha, Complete magnetization reversal in a magnetostrictive nanomagnet with voltage-generated stress: A reliable energy-efficient non-volatile magneto-elastic memory, *Appl. Phys. Lett.* **105**, 072408 (2014).
- [23] A. K. Biswas, S. Bandyopadhyay, and J. Atulasimha, Experimental demonstration of complete 180° reversal of magnetization in isolated Co nanomagnets on a PMN-PT substrate with voltage generated strain, *Nano Lett.* **17**, 3478 (2017).
- [24] K. Roy, S. Bandyopadhyay, and J. Atulasimha, Binary switching in a symmetric potential landscape, *Sci. Rep.* **3**, 3038 (2013).
- [25] H. Q. Cui, L. Cai, X. K. Yang, S. Wang, C. W. Feng, L. Xu, and M. L. Zhang, Voltage pulse induced repeated magnetization reversal in strain-mediated multiferroic nanomagnets: A size- and material-dependent micromagnetic study, *J. Phys. D: Appl. Phys.* **50**, 285001 (2017).
- [26] R. Matsumoto, T. Nozaki, S. Yuasa, and H. Imamura, Voltage-Induced Precessional Switching at Zero-Bias Magnetic Field in a Conically Magnetized Free Layer, *Phys. Rev. Appl.* **9**, 014026 (2018).
- [27] J. H. Liu, X. K. Yang, H. Q. Cui, B. Wei, C. Li, Y. B. Chen, M. L. Zhang, C. Li, and D. N. Dong, Voltage pulse-induced fast and repeated switching in a uniaxial nanomagnet at room temperature, *J. Magn. Magn. Mater.* **491**, 165607 (2019).
- [28] R. Matsumoto and H. Imamura, Low-Power Switching of Magnetization Using Enhanced Magnetic Anisotropy with Application of a Short Voltage Pulse, *Phys. Rev. Appl.* **14**, 021003 (2020).
- [29] O. Kovalenko, T. Pezeril, and V. V. Temnov, New Concept for Magnetization Switching by Ultrafast Acoustic Pulses, *Phys. Rev. Lett.* **110**, 266602 (2013).
- [30] C. C. Zhu, C. Li, Y. B. Chen, J. H. Liu, and L. Fang, Strain manipulation of vortex core in bi-component magnetic nanodisks, *J. Phys. D: Appl. Phys.* **54**, 495001 (2021).
- [31] B. D. Cullity and C. D. Graham, *Introduction to Magnetic Materials* (Wiley, New York, 2009).
- [32] J. Fidler and T. Schrefl, Micromagnetic modelling - the current state of the art, *J. Phys. D: Appl. Phys.* **33**, 135 (2000).
- [33] A. Vansteenkiste, J. Leliaert, M. Dvornik, M. Helsen, F. Garcia-Sanchez, and B. V. Waeyenberge, The design and verification of MuMax3, *AIP Adv.* **4**, 107133 (2014).
- [34] J. H. Liu, X. K. Yang, D. H. Hong, C. Li, N. Xu, B. B. Yang, and L. Fang, Voltage manipulation of desired magnetization orientation in multiferroic heterostructures, *Scr. Mater.* **193**, 132 (2021).
- [35] R. Alben, J. J. Becker, and M. C. Chi, Random anisotropy in amorphous ferromagnets, *J. Appl. Phys.* **49**, 1653 (1978).
- [36] A. Manzin and R. Ferrero, Control of vortex chirality in bi-component magnetic nanodisks, *Appl. Phys. Lett.* **115**, 042402 (2019).
- [37] W. F. Brown, Thermal fluctuations of a single-domain particle, *J. Appl. Phys.* **34**, 1319 (1963).
- [38] J. Leliaert, J. Mulkers, J. De Clercq, A. Coene, M. Dvornik, and B. Van Waeyenberge, Adaptively time stepping the stochastic Landau-Lifshitz-Gilbert equation at nonzero temperature: Implementation and validation in MuMax3, *AIP Adv.* **7**, 125010 (2017).
- [39] D. C. Vaz, *et al.*, in *2021 IEEE International Electron Devices Meeting (IEDM)*, 32.4.1 (2021).
- [40] M. A. Abeed and S. Bandyopadhyay, Experimental demonstration of an extreme subwavelength nanomagnetic acoustic antenna actuated by spin-orbit torque from a heavy metal nanostrip, *Adv. Mater. Technol.* **5**, 1901076 (2020).
- [41] N. D'Souza, M. S. Fashami, S. Bandyopadhyay, and J. Atulasimha, Experimental clocking of nanomagnets with strain for ultralow power Boolean logic, *Nano Lett.* **16**, 1609 (2016).
- [42] J. Leliaert, B. Van de Wiele, A. Vansteenkiste, L. Laurson, G. Durin, L. Dupré, and B. Van Waeyenberge, A numerical approach to incorporate intrinsic material defects in micromagnetic simulations, *J. Appl. Phys.* **115**, 17D102 (2014).
- [43] D. Toscano, S. A. Leonel, P. Z. Coura, F. Sato, R. A. Dias, and B. V. Costa, Dynamics of the vortex core in magnetic nanodisks with a ring of magnetic impurities, *Appl. Phys. Lett.* **101**, 252402 (2012).
- [44] N. Del-Valle, J. Castell-Queralt, L. González-Gómez, and C. Navau, Defect modeling in skyrmionic ferromagnetic systems, *APL Mater.* **10**, 010702 (2022).
- [45] A. K. Biswas, J. Atulasimha, and S. Bandyopadhyay, The straintronic spin-neuron, *Nanotechnology* **26**, 285201 (2015).
- [46] S. Nasrin, J. L. Drobitch, S. Bandyopadhyay, and A. R. Trivedi, Low power restricted Boltzmann machine using mixed-mode magneto-tunneling junctions, *IEEE Electron Device Lett.* **40**, 345 (2019).
- [47] Y. B. Chen, B. Wei, X. K. Yang, J. H. Liu, J. Li, H. Q. Cui, C. Li, and M. X. Song, In-plane magnetization switching characteristics of energy-efficient strain-mediated nanomagnets assisted by the spin Hall effect at room temperature, *J. Magn. Magn. Mater.* **514**, 167216 (2020).
- [48] J. H. Yuan, X. K. Yang, B. Zhang, Y. B. Chen, J. Zhong, B. Wei, M. X. Song, and H. Q. Cui, Activation function and computing performance of spin neuron driven by magnetic field and strain, *Acta Phys. Sin.* **70**, 207502 (2021).
- [49] J. H. Yuan, Y. B. Chen, S. Q. Dou, B. Wei, H. Q. Cui, M. X. Song, and X. K. Yang, Pure voltage-driven spintronic neuron based on stochastic magnetization switching, *Nanotechnology* **33**, 155201 (2021).
- [50] Y. LeCun, C. Cortes, and C. J. C. Burges, The MNIST Database of handwritten digits, <http://yann.lecun.com/exdb/mnist/>.
- [51] J. H. Liu, T. Xu, H. M. Feng, L. Zhao, J. S. Tang, L. Fang, and W. J. Jiang, Compensated ferrimagnet based artificial synapse and neuron for ultrafast neuromorphic computing, *Adv. Funct. Mater.* **32**, 2107870 (2022).